SAND--82-2887

DE84 014308

SAND82-2887
Unlimited Distribution
Printed January 1983

IMPROVED ATOMIC DATA FOR ELECTRON-TRANSPORT PREDICTIONS BY THE CODES TIGER AND TIGERP: I. INNER-SHELL IONIZATION BY ELECTRON COLLISION

James M. Peek
Theoretical Division 1231

John A. Halbleib
Theoretical Division 1231

Sandia National Laboratories
Albuquerque, New Mexico 87185

Abstract

The inner-shell ionization data for electron-target collisions now in use in the TIGER and TIGERP electron-transport codes are extracted and compared with other data for these processes. The TIGER cross sections for K-shell ionization by electron collisions are found to be seriously in error for large-Z targets and incident electron energies greater than 1 MeV. A series of TIGER and TIGERP runs were carried out with and without improved K-shell electron ionization cross section data replacing that now in use. The relative importance of electron-impact and photon ionization of the various subshells was also extracted from these runs. In general, photon ionization dominated in the examples studied so the sensitivity of many predicted properties to errors in the electron-impact subshell ionization data was not large. However, some differences were found and, as all possible applications were not covered in this study, it is recommended that these electron-impact data now in TIGER AND TIGERP be replaced. Cross section data for the processes under study are reviewed and those that are most suitable for this application are identified.

DISCLAIMER

I. Introduction

The TIGER[1], TIGERP[2], and other closely related Sandia codes have a history of successful applications to many problems in electron and photon transport. They utilize a MONTE CARLO approach to the solution of the transport problem[3] and a large quantity of collision data for electron/photon interactions with the target material is required in this process[4,5]. The quality of these data is always of concern[6,7] since a complete set with a documented accuracy will never be available. For this reason, the electron ionization cross sections for the inner-shells of atomic targets are reconsidered here in some detail.

The choice of these particular mechanisms is also motivated by additional factors. First, weaknesses in the inner-shell ionization cross sections by electron impact were identified in an earlier study of the atomic-physics data used in these codes[6]. Second, an increased need to follow the transport of relatively low-energy electrons and photons emphasizes the importance of these physical processes. For example, attempts to provide a better spatial definition for charge and energy deposition obviously increases the demands on describing the behavior of low-energy electrons. Many of these low-energy electrons are higher-generation particles produced in direct

ionization events or in the decay of inner-shell vacancies produced by these ionization events. Also, fluorescence produced in the relaxation of the inner-shell vacancies can have an influence on the photon spectrum predicted for energies less than about 50 keV.

The importance of the inner-shell electron ionization cross sections is assessed for a limited class of problems. A typical bremsstrahlung-converter problem is treated with both the TIGER and TIGERP codes. This problem is discussed in some detail. The discussion is intended to display data that can be useful in analyzing transport problems not considered here as well as documenting the present study.

The TIGER code treats only ionization from the K shell while TIGERP considers the K, L, and M shells. The electron ionization cross section for the K shell is different in the two codes. In addition, data based on yet a third cross section for electron ionization of the the K shell are analyzed. Differences in the strength of the predicted K-shell fluorescence lines are observed and these differences are related to the electron ionization cross sections used in the two codes. The TIGERP code also predicts fluorescence photons and Auger electrons from the relaxation of the L and M shells which is necessarily ignored in the TIGER code. These differences are quantified. In summary, these two codes are observed to predict identical continuum, or bremsstrahlung, radiation

spectra for the cases studied with all differences limited to the properties of the line spectra just discussed. Furthermore, the emitted line radiation appeared to be relatively insensitive to changes in the electron K-shell ionization cross section.

Inner-shell vacancies are produced both by electron and by photon collisions with the target. For incident electron energies of a few MeV or less, those energies of primary interest here, the secondary electrons may come from low- to high-generation processes and the photons are created mainly by bremsstrahlung collisions of the primary electrons with the target. The relative importance of the electron versus photon vacancy production is studied, and data for the various subshells as a function of incident energy is presented. The production of vacancies by photon collisions tends to dominate the electron-collision process for the K shell while the reverse is true for the L and M shells.

The rather large differences found here for the inner-shell electron ionization cross sections in use, both in comparison with various theoretical results and in comparison with experiment, lead to the conclusion that these data in TIGER and TIGERP should be replaced. Admitting that no great sensitivity to these cross sections was observed in the studies presented here, the inadequacies of these cross sections is so great that any other transport study involving different parameters would have to

reconsider this sensitivity analysis. The preventative maintenance approach seems to be the most efficient solution given the relative ease with which these data can be replaced.

The requirements of the electron/photon transport problem, such as the need for the relevant cross section from threshold to relativistic collision energies for all atoms in the periodic table and the need to have these data in compact and convenient form, are used to evaluate the data now available. One particular set of cross-section data seems best suited for this application and it is recommended that these data be incorporated into the TIGER/TIGERP series of transport codes.

The following section presents the electron-transport data found in the examples studied here as well as the various cross section data extracted from the TIGER series of codes. The third section presents a critical review of the available data for inner-shell ionization by electron collision. The fourth and last section summarizes the findings presented here and presents the recommendations for improvements in Sandia's electron/photon transport code data base.

II. TIGER/TIGERP Spectra For Bremsstrahlung Converters

There are any number of electron/photon transport problems that could be used to test the electron ionization cross sections in use for the various subshells. The bremsstrahlung converter problem is chosen not so much because it is believed to be sensitive to these processes as for the fact that this problem has been of considerable interest to Sandia's activities. Hence, this choice will provide some insight into past and future applications. The target is taken as a layer of tantalum (Z=73) with a back layer of carbon. These materials are assumed to be of normal density with a thickness of roughly one-third range in the tantalum and two-thirds range in the carbon, and the monoenergetic electrons are perpendicularly incident on the tantalum layer.

The reflected photon spectrum for 0.35 MeV incident electrons is shown in Fig. 1 for TIGER and TIGERP. The continuum spectra are almost always within statistical uncertainties. This is expected since the data concerned with generating this spectra are virtually identical in the two codes. The only differences are related to the treatment of the photon and electron ionization of the target's inner shells and the subsequent relaxation of those shells.

The photoionization cross sections are the same in the two codes, while the K-shell electron ionization cross section is that of Authors and Moiseiwitsch (AM)[8] in TIGER and Gryzinski (G)[9] in TIGERP. These same cases have been run with the AM electron ionization cross section replaced by that of Kolbenstvedt (KV)[10] in TIGER. The TIGER code also treats the K-shell fluorescence spectrum as a single line while the TIGERP code splits this line into the components indicated by Fig. 2, which shows details omitted in Fig. 1. The TIGER code does not consider other inner-shell processes, so fluorescence and Auger transitions from these higher shells are necessarily omitted. The TIGERP code treats the K- and L-shell transitions indicated in Fig. 2. The minor differences resulting from these two treatments can be seen in Fig. 1.

The transmitted intensity of the K-shell fluorescence line resulting from using the KV cross section in TIGER, not shown in Figs. 1 or 2, is larger than that found with the AM cross section by about 3%, which is just larger than the statistical uncertainties in this calculation. This agreement can be seen to be to a large extent fortuitous by inspecting Fig. 3. The K-shell ionization cross sections used in these calculations are shown as a function of collision energy, E, and AM agrees well with KV only in the $0.2 < (E/MeV) < 0.8$ range. Since AM is smaller than KV for $E < 0.2$ MeV and this energy range can play a minor role in

this 0.35 MeV example, the cross sections shown in Fig. 3 and the K-shell intensity differences seem consistent. The sum of the energy in the transmitted K-shell lines predicted by TIGERP, which uses the G electron ionization cross section, is smaller than the TIGER/KV results by about 10% and this result also appears to be explained by the cross section differences shown in Fig. 3.

The transmitted L- and M-line spectrum predicted by TIGERP is relatively weak in this example because of the strong self-absorption of these longer wave-length photons. Their contributions are more than an order of magnitude less than that of the K shell lines, hence their neglect is of little consequence compared to the total transmitted radiation energy. They are more important in the reflected spectra, as shown in Figs. 1 and 2. The total reflected energy in the lines is about 12% of the total and that of the L and M shells is 2%.

A summary of the photon energies resulting from inner-shell radiative-relaxation processes for tantalum and the associated reflected line intensities for the example treated here is given in Table I. The total reflected photon number and energy from TIGERP are 0.0293 (1) and 0.00531 (1) MeV per source electron, respectively. The corresponding results from the TIGER calculation are 0.0256 (2) and 0.00520 (1) MeV per source electron. Here and in Table I the numbers in parentheses are the estimated

one-sigma statistical uncertainties expressed as percents of the given quantities.

The above data and other data not reported here suggest that the x-ray spectra from a bremsstrahlung converter is not particularly sensitive to the electron ionization cross sections. To further explore this point the total number of ionization events that lead to the production of an inner-shell hole was extracted and partitioned into the contributions from electron-impact and photon ionization. The ratio of the electron events to the total number for the K-shell is shown in Fig. 4 as a function of incident electron energy for the target described earlier. The effects of the G, KV, and AM cross sections are also displayed. (The analogous ratio for photon ionization is obtained by subtracting the electron ratio from unity.)

The differences in the various electron K-shell ionization cross sections, shown in Fig. 3, are clearly related to the data shown in Fig. 4. Of most interest, the G cross section is the smallest of those tested for $E < 3$ MeV and the corresponding ratio shown in Fig. 4 is also the smallest for incident energies less than 3 MeV. A similar relationship exists for the largest, KV, cross section. The results based on the AM cross section show the interesting property of approaching the KV ratio for small incident energies while decreasing more rapidly with increasing incident energy until it becomes smaller than the G ratio

for E near 50 MeV. These trends again reflect the relationships between the K-shell electron ionization cross sections shown in Fig. 3.

Figure 4 shows the dominance of photon events for incident energies greater than 1.0 MeV. Electron events start to become more important for smaller incident energies, and this is undoubtedly related to the reduction of the bremsstrahlung production with decreasing E. A decrease in the sensitivity of the K-shell fluorescence line(s) emitted from the target to the electron ionization cross section with increasing incident energy is implied, and was observed in calculations not reported here.

The behavior of the L and M shell vacancy production is quite different. In these cases, electron collision events dominate for all E. About 86% of the L-shell events are due to electrons for the 0.35 MeV incident energy case, with a decrease to 78% at 35 MeV. M-shell ionization events are about 97% due to electron collisions and this factor is independent of E for the range considered in Fig. 4. The reason for this behavior is qualitatively explained by the rough scaling laws[6] for the electron ionization cross section, which have it directly proportional to the number of electrons in the subshell and inversely proportional to the square of the binding energy of the subshell.

No information on the Z dependence of this or other problems has been provided in this discussion. Qualitative arguments could be presented, but efforts to isolate a transport problem that is seriously effected by errors in the electron impact ionization cross section would appear to serve little purpose. The essential result is that these cross sections obtained from the TIGER and TIGERP codes differ greatly in certain collision energy ranges. Hence, the following arguments are devoted to the detailed analysis of the cross sections themselves.

III. Innershell Electron-Impact Cross Sections

The collision energy and Z dependence of the electron-impact cross sections for the K, L and M shells are now discussed. The intent is to establish a value judgement on the cross sections now in use and to identify data improvements that can conceivably be incorporated into Sandia's transport codes.

Figure 3 shows two other ionization cross sections for the K shell of Ta in addition to those that have been implemented in the TIGER and TIGERP codes. These data reflect a number of properties that have been previously identified. See, for example, Refs. 6 and 11. The G cross section has received considerable attention because of its simplicity. Its most successful application has been to the ionization of the K-shell, although it never seems to fail dramatically. The essential problems with the G cross section have been identified with it being too small in the large collision-energy region[11] and not having the correct relativistic singularity at $v/c = 1$, where v is the relative collision velocity and c is the speed of light[6]. These two problems are not unrelated and are reflected in Fig. 3 by the fact that G is smaller than all but the AM cross section in the large collision energy region.

The AM cross section has been discussed thoroughly elsewhere[6] where it was made clear that this cross section should not be applied to targets with Z > 30 or used for E larger than 20 times the K-shell ionization energy, as recommended by the authors of Ref. 8. Hence, the pathological behavior of the AM cross section for this Z = 73 and E > 1 MeV case is no surprise. the correct high-energy behavior is exhibited by the Schofield (S)[12], Ref. 10(KV), or the Ref. 13(P) cross sections. The general agreement of the AM cross section with the other data in the threshold region could not be anticipated.

The KV cross section is simple, and therefore popular, and has proved successful in the high energy region[6]. The KV data obtained from TIGER for this case shows, however, somewhat unusual behavior for small E, which displays its greatest weakness[6]. In addition, the small slope shown in Fig. 3 in the high-energy range, as compared with the S and P data, is considered a weakness[13].

The S data are based on relativistic first-Born theory and represent the most comprehensive tabulation in the high-energy region and one of the most sophisticated of its type (many calculations of comparable accuracy are available for a limited selection of targets[6]). The lack of data in the threshold region is a serious limitation. Also, the disagreement with the G data at the lowest values of E for which there are data for this cross section is a troublesome

point since the G data tend to be reasonable[11] in this intermediate E range.

The Ref. 13 data are based on the relativistic extension of calculations by McGuire[14]. These data have been studied extensively in the non-relativistic region of E by their author and reasonable accuracy is claimed. The general agreement with the G data shown in Fig. 3 for the threshold region is therefore expected. The fact that the P cross section is larger than either the S or KV predictions for high energy is expected[13] and the difference shown here is not considered serious in light of the generally good agreement with experiment found for other targets in the high-energy region[13,14].

An example of electron ionization of the L subshells of gold is shown in Fig. 5. The general agreement of the S and G theoretical predictions with experiment is impressive for this case. However, the tendency for G to be too low is clearly evident for the threshold and high-energy regions. The P data are too large by about 25% for one case shown in Fig. 5, but it is the best theory for spanning the threshold to high-energy region. There are no other theoretical data for this ionization cross section that systematically cover the large Z and E ranges required in this application.

Figures 6-8 show data similar to that of Fig. 5 for the ionization of the L subshells of xenon. In these cases, the G and P cross sections agree well with experiment, which are

only available in the near-threshold region. The S data do not extend to sufficiently low E values to be compared with experiment but, for reasons explained above, they represent what is arguably the best available in the high-energy region. The tendency of the G theory to be too small for high energy is evident, if the preceding statement is accepted. Again, the Ref. 13 data seem to best span the entire energy region.

Figure 9 shows the few data available for the ionization of the M shell of a relatively large-Z target; Z = 79 to be specific. Here, the one experimental measurement lies 30% or more above the G and P cross sections. These two theoretical cross sections are in remarkably good agreement except at high energy, where the G data become, again, smaller than the P data.

IV. Conclusions

Section III presented a number of examples and some discussion that displays the properties and accuracy estimates for a number of theoretical cross sections for the electron-impact ionization of atomic subshells. The emphasis on theory is made necessary both because of the fragmentary experimental data base and the requirement that the cross sections be represented in as compact a form as is possible. The latter requirement is imposed by digital-computer limitations.

Table II is an attempt to represent this discussion in a compact form. The information concerning the subshells, E ranges, and targets for which there are data are undisputable facts. The accuracy estimates are another matter. The present approach has been to assume the accuracy is acceptable (+) if no major flaw has been identified. If a major flaw has been found, an unacceptable (-) rating results.

Introducing a quantified ranking system does not remove the subjective nature of these decisions. For example, the use of first Born theory for ionization in the threshold E range is questioned by many, while much recent experience indicates this approach is useful, see Ref. 15 for an example. Additional questions of this type will not be raised here.

The following three recommendations, which can be implemented separately, are made: 1. The limitations of the AM cross section for K-shell ionization by electron collisions are such that it should be replaced in TIGER. The cross sections from Refs. 9, 10, and 13 satisfy the objective requirements listed in Table II and the Ref. 13 data offer a slight advantage in accuracy, as discussed in Sec. III. It is estimated that the change to Ref. 9 (G) or to Ref. 10 (KV) cross sections in TIGER would require no more than a week for one individual. The estimate for installing the Ref. (13) cross sections is one-to-two months for one individual. 2. The shortcoming of the G cross sections at large E is serious from the point of view that extremely large differences from better founded theories occur (see Fig. 3). More accurate data are available from Ref. 13 for the high-energy behavior that also has other advantages. See Table II. Hence, it is recommended that the Ref. 9 (G) cross sections in TIGERP be replaced by the Ref. 13 cross sections. The estimate for doing this work is three-to-four months for one individual. 3. Any number of combinations of these data could be used to replace the worst aspects of a particular cross section. For example, the problems of the G cross section at high energy could be mitigated by "patching" it to a good high-energy theory such as that of Ref. 12. Reference 12 does not provide data for M shell ionization, but the results from Ref. 13 could be

used for this case. This recommendation is of value only if there is a strong objection to the previous two recommendations and if there is a strong predisposition for using a particular cross section. An estimate for including any such cross section in TIGER or TIGERP can be derived from the estimates given above provided a suitable increase is included to accommodate any complexities introduced by the "patching" procedure.

References

1. J. A. Halbleib and W. H. Vandevender, Nucl. Sci. Eng. 57, 94 (1975).

2. J. A. Halbleib, Sr., and J. E. Morel, Nuc. Sci. Eng. 70, 219 (1979).

3. M. J. Berger, "Monte Carlo Calculation of the Penetration and Diffusion of Fast Charged Particles". Methods in Computational Physics, Vol. 1, Ed. by B. Alder, S. Fernbach, and M. Rotenberg, (Academic, New York, 1963).

4. M. J. Berger and S. M. Seltzer, "Electron Monte Carlo Programs, I. Introduction and Notes on Program DATPAC 4", National Bureau of Standards Report 9836, (1968).

5. H. M. Colbert, "A Computer Program for Calculating Combined Photon-Electron Transport in Complex Systems," Sandia Laboratories Report SCL-DR-72-109 (1974).

6. J. M. Peek, "Cross Sections for Electron and Photon Processes Required by Electron-Transport Calculations," Sandia Laboratories Report SAND79-0772 (1979).

7. S. M. Seltzer and M. J. Berger, Trans. Am. Nucl. Soc. 41, 477 (1982),

8. R M. Authors and B. L. Moiseiwitsch, Proc. Roy. Soc. A 247, 550 (1958).

9. M. Gryzinski, Phys. Rev. 138, A336 (1965).

10. H. Kolbenstvedt, J. Appl. Phys. 38, 4785 (1967).

11. C. J. Powell, Rev. Mod. Phys. 48, 33 (1976).

12. J. H. Scofield, Phys. Rev. A, 18, 963 (1978).

13. J. M. Peek, (unpublished).

14. E. J. McGuire, J. de Physique, 32, C4-37 (1971); E. J. McGuire, Phys. Rev. A, 16, 73 (1977).

15. See S. M. Younger, Phys. Rev. A22, 111 (1980) and the references cited in this paper for examples.

16. J. Palinkas and B. Scklenk, Z. Physik A, 297, 29 (1980).

17. K. Shima, T. Nakagawa, K. Umetani, and T. Mikumo, Phys. Rev. A, 24, 72 (1981).

18. R. Hippler, I. McGregor, M. Aydinol, and H. Kleinpoppen, Phys. Rev. A, 23, 1730 (1981).

19. J. Palinkas and B. Schlenk, J. Phys. B, 13, 1631, (1980).

Table I. Line energies for tantalum and the intensities of the reflected lines for the case discussed in Sec. II are shown. The notation for the transitions is defined in the caption to Fig. 2. All entries but the last are for TIGERP and the last is for the single line treated in TIGER. The numbers in parentheses are the estimated one-sigma statistical uncertainties expressed as percents of the given quantity.

Transition	Energy(keV)	(Number/electron)*1000
$\langle\bar{M}\rangle$	1.9298	0.119 (40)
$L_{III}\bar{M}$	8.1352	1.78 (2)
$L_{II}\bar{M}$	9.3189	1.19 (3)
$L_{I}\bar{M}$	9.3816	0.340 (2)
$\langle L_{III}\rangle$	9.8810	0.188 (5)
$\langle L_{II}\rangle$	11.1360	0.0884 (3)
$\langle L_{I}\rangle$	11.6800	0.0442 (6)
$\alpha_2 KL_{II}$	56.2780	0.924 (2)
$\alpha_1 KL_{III}$	57.5330	1.72 (2)
$K\bar{M}$	65.2405	0.596 (2)
$\langle K\rangle$	67.4140	0.0939 (2)
$\langle\bar{K}\rangle$(TIGER)	58.8700	3.68 (1)

Table II. Summary of available data and an accuracy evaluation for the cross sections discussed in Sec. III. The threshold ionization energy is indicated by I. The indicated data are sufficiently accurate for the present application if a + appears and either it does not exist or it is not sufficiently accurate if a - appears.

Cross Section	Shells Available	Missing E Range	Missing Targets	Accuracy in Given E Ran Low	Intermediate	Lar
Ref. 8	K	E>20*I	Z>30	+	+	+
Ref. 9	all	none	none	+	+	-
Ref. 12	K, L_I, L_{II}, L_{III}	I region	none	-	+	+
Ref. 10	K	none	none	_	+	+
Ref. 13	all	none	none	+	+	+

Figure Captions

1. The reflected photon spectrum for 0.35 MeV electrons perpendicularly incident on a tantalum target is displayed as a histogram. The tantalum is normal density and is one-third range in thickness for 0.35 MeV electrons. A layer of carbon at normal density and two-thirds of a range thick is on the back side of the target. The number of photons per MeV reflected for each incident electron is shown as a function of photon energy in MeV. The broken line represents TIGER data and the solid line TIGERP data. The vertical lines represent subshell fluorescence spectra. The numbers near each line in this and in Fig. 2 give their height. The line at about 0.002 MeV is the average M-shell, symbolized by $\bar{M}$, fluorescence as treated by TIGERP. The group near 0.01 MeV are from the L-shell fluorescence predicted by TIGERP, and the group near 0.6 MeV are K-shell fluorescence from both TIGER and TIGERP.

2. The data shown in Fig. 1 are repeated on an expanded energy scale to show more detail. The numbers indicate the height for that line. Standard spectroscopic notation identifies each line when possible. Otherwise, the symbols indicate the upper and lower states for that transition. The quantities in < > indicate a transition between the indicated state and some typical excited state, with a transition energy equal to the binding energy of the indicated state and transition probabilities determined from normalization requirements. See Ref. 3 for more details concerning the treatment of the inner-shell relaxation processes.

3. The cross section for the electron-impact ionization of the K-shell of tantalum is shown as a function of electron collision energy. Curve 1 is from TIGER, using Ref. 8 (AM) ionization data, and curve 2 is from TIGERP, using Ref. 9 (G) ionization data. Curve 4 was generated in TIGER after the AM cross section had been replaced by the Ref. 10 (KV) cross section. Curve 3 is from Ref. 12 and curve 5 is from Ref. 13.

4. The fraction of K-shell ionization events due to electron-impact ionization is shown as a function of the energy of the incident monoenergetic beam. The fraction of K-shell ionization events due to photon ionization is one minus the number given in this graph. The solid curve is from TIGERP and is based on the G cross section. The broken curve is from TIGER using the AM cross section and the dot-dash curve is from TIGER using the KV cross section.

5. Cross sections for the ionization of the L subshells in Au are shown as a function of the electron collision energy. The solid squares, triangles, and circles are experimental data from Ref. 16 for the L_I, L_{II}, and L_{III} levels. The open squares are experimental data from Ref. 17 for the L_{III} level. The solid curves are from Ref. 13, with the upper curve for L_{III} and the lower for L_{II} ionization. The L_I cross section from Ref. 13, not shown, is about 5% lower than the L_{II} curve. The remaining theoretical curves, ordered as $L_{III} > L_{II} > L_I$, are from Ref. 12, broken curves, and Ref. 9 as calculated in TIGERP, dot-dash curve.

6. Cross sections for the ionization of the L_I subshell in xenon are shown as a function of electron collision energy. The open circles are experimental data from Ref. 18, the upper solid curve is from Ref. 13, the lower solid curve, from Ref. 14, is the nonrelativistic equivalent to the upper solid curve, the broken curve is from Ref. 12, and the dot-dash curve represents data generated in TIGERP when the Ref. 9 cross section is used.

7. Same as Fig. 6 except these data are for the L_{II} subshell of xenon and the Ref. 10 curve is not shown.

8. Same as Fig. 6 except these data are for the L_{III} subshell of xenon and the Ref. 10 curve is not shown.

9. Cross sections for the ionization of the M shell of Au are shown as a function of electron collision energy. All M sub-levels have been averaged in these data. The experimental points are from Ref. 19. The solid curve is from Ref. 13 and the dot-dash curve represents data generated in TIGERP when the Ref. 9 cross section is used.

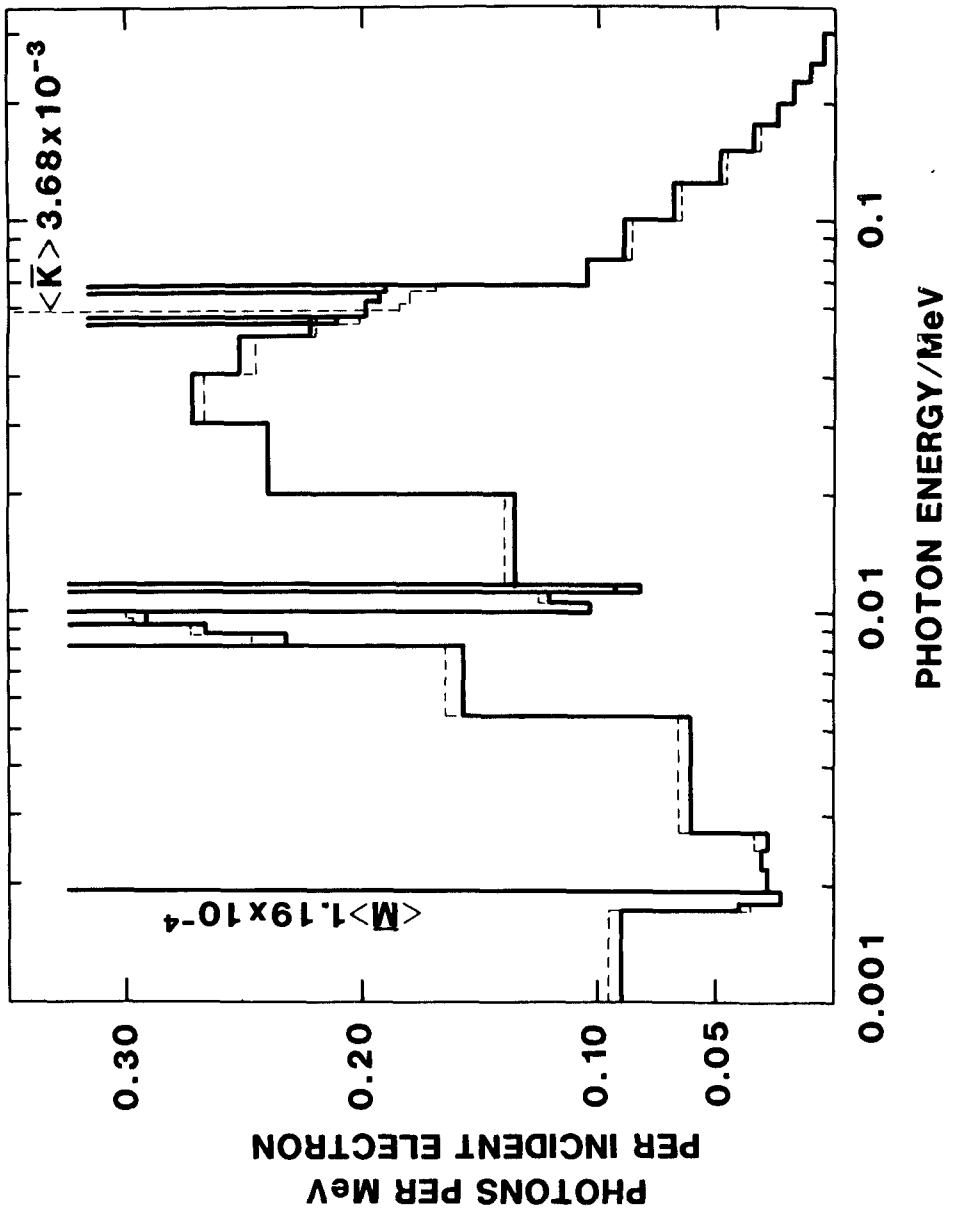
$\langle \bar{K} \rangle 3.68 \times 10^{-3}$
$\langle \bar{M} \rangle 1.19 \times 10^{-4}$
0.1
0.01
0.001
PHOTON ENERGY/MeV
0.30
0.20
0.10
0.05
PHOTONS PER MeV
PER INCIDENT ELECTRON

Fig. 1

PHOTONS PER MeV PER INCIDENT ELECTRON
0.40
0.35
0.30
0.25
0.20
0.15
0.10
0.05
0.008
0.009
0.010
0.6
0.7
PHOTON ENERGY/MeV
$L_{III}\bar{M}$ 1.78x10^{-3}
$L_{II}\bar{M}$ 1.19x10^{-3}
$L_{I}\bar{M}$ 3.40x10^{-4}
$<L_{III}>$1.88x10^{-4}
$<L_{II}>$8.84x10^{-5}
$<L_{I}>$4.42x10^{-5}
α_2 KL$_{II}$ 9.24x10^{-4}
α_1 KL$_{III}$ 1.72x10^{-3}
K$\bar{M}$ 5.96x10^{-4}
<K> 9.39x10^{-5}

Fig. 2

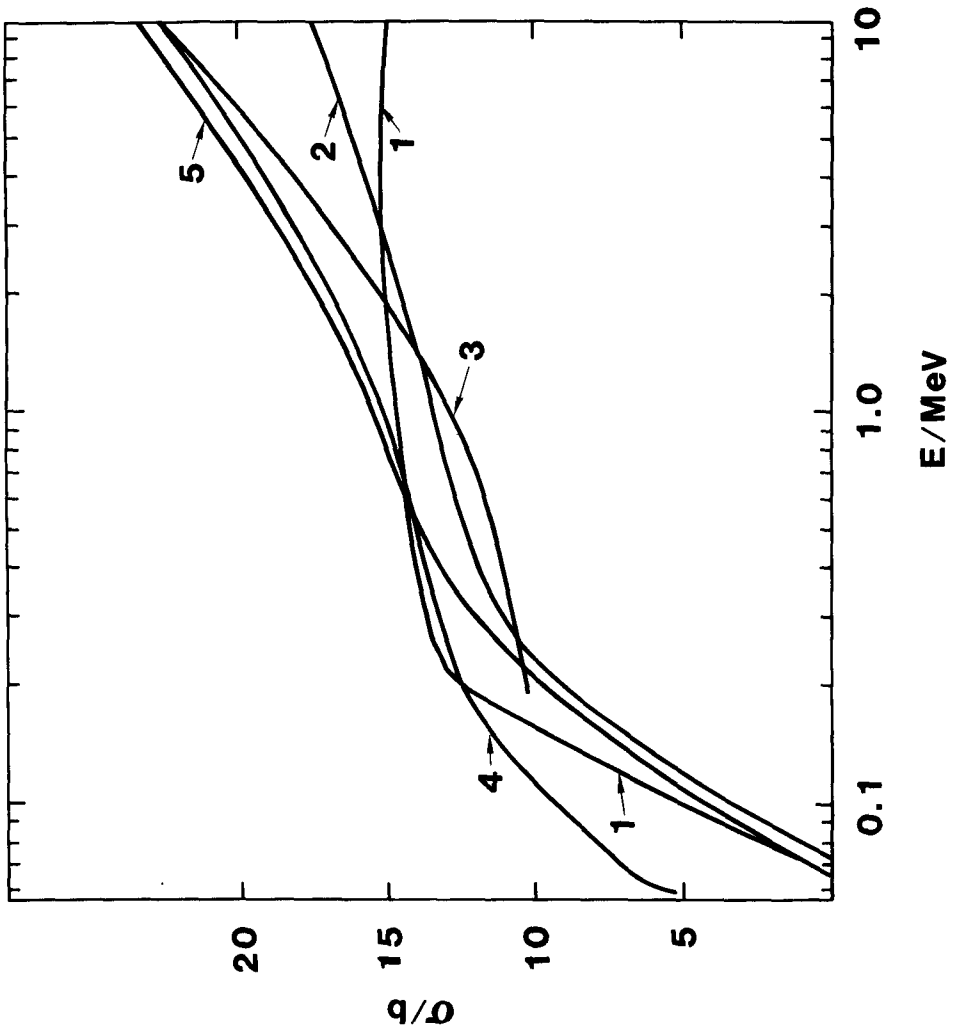

Fig. 3

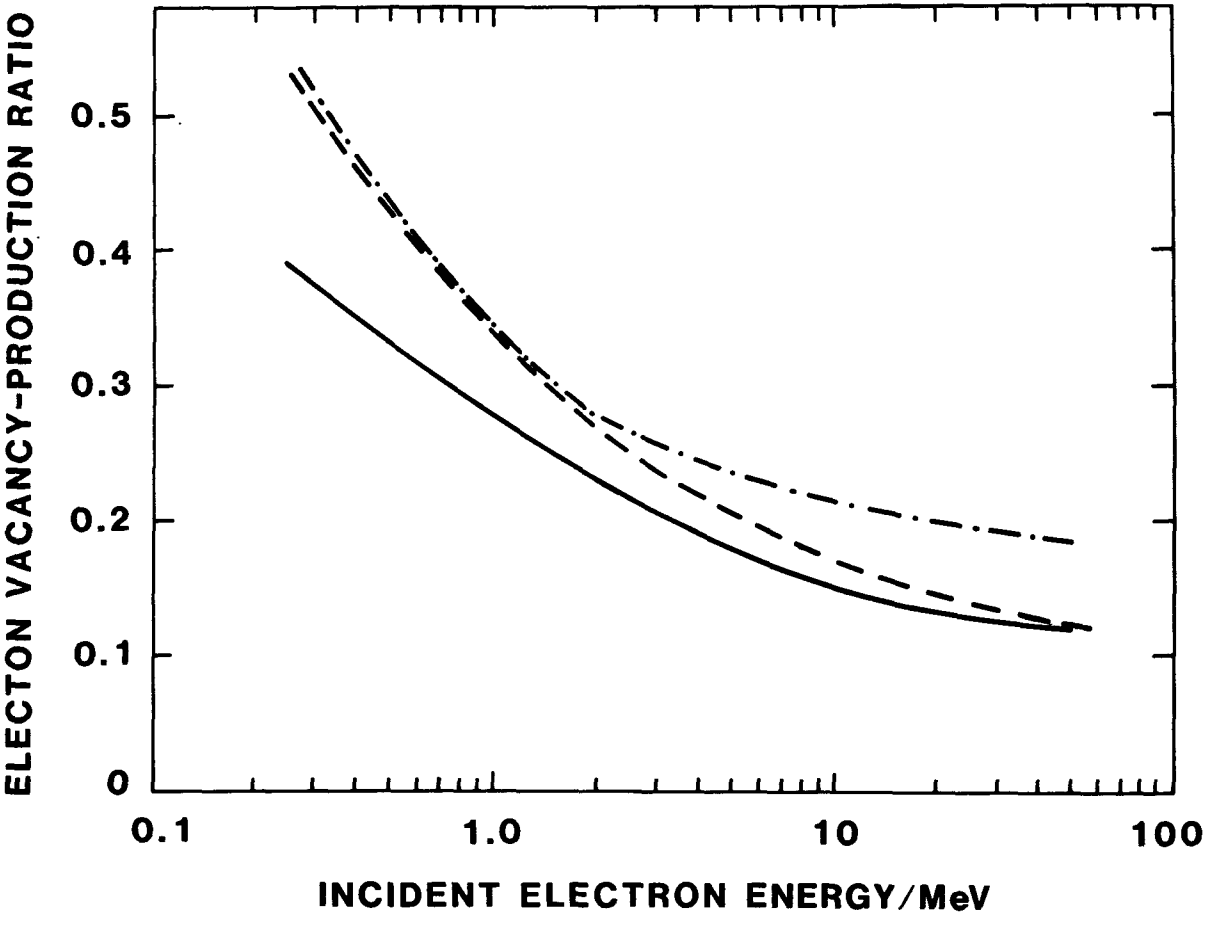
ELECTON VACANCY-PRODUCTION RATIO
0.5
0.4
0.3
0.2
0.1
0
0.1
1.0
10
100
INCIDENT ELECTRON ENERGY/MeV

Fig. 4

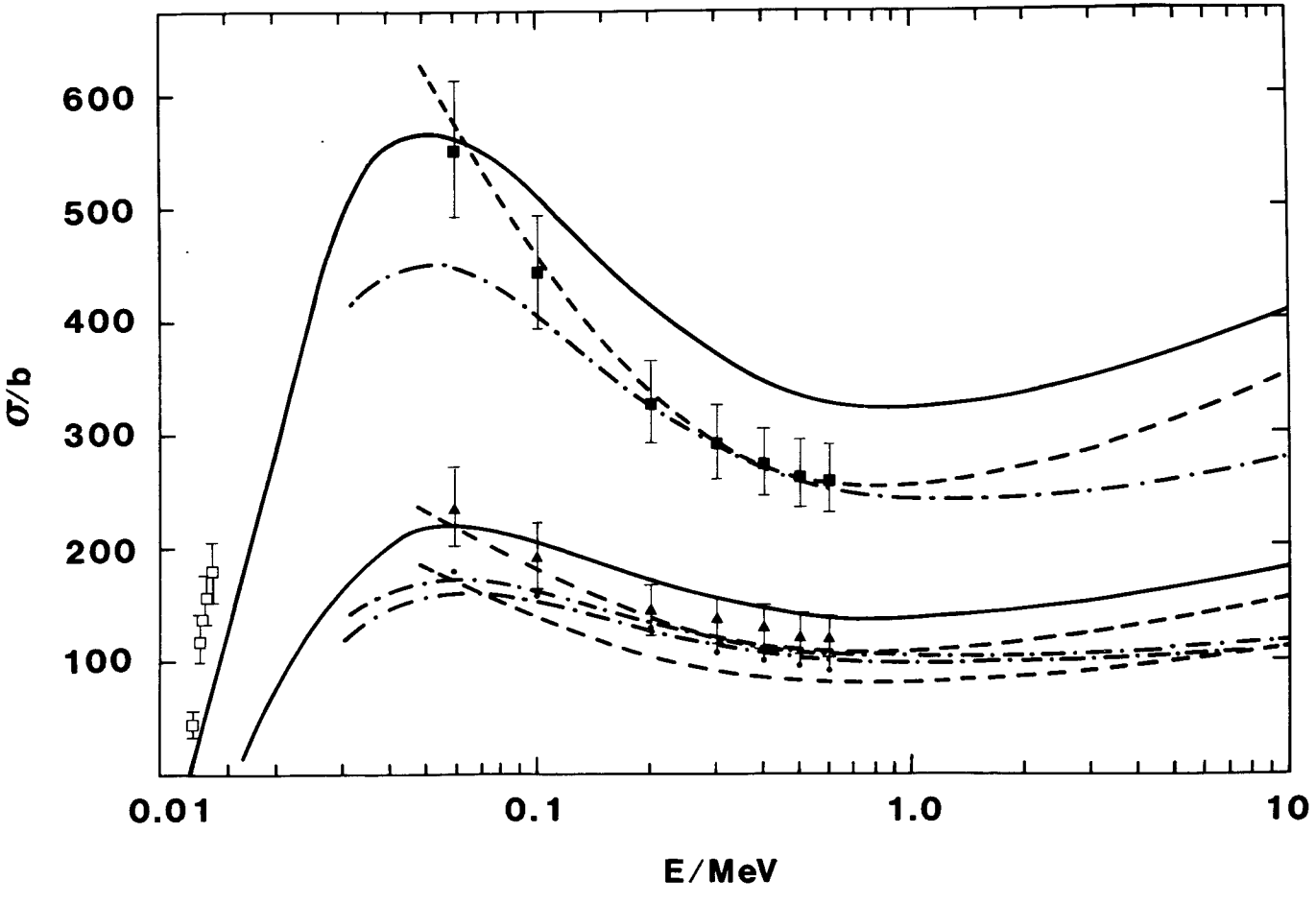

Fig. 5

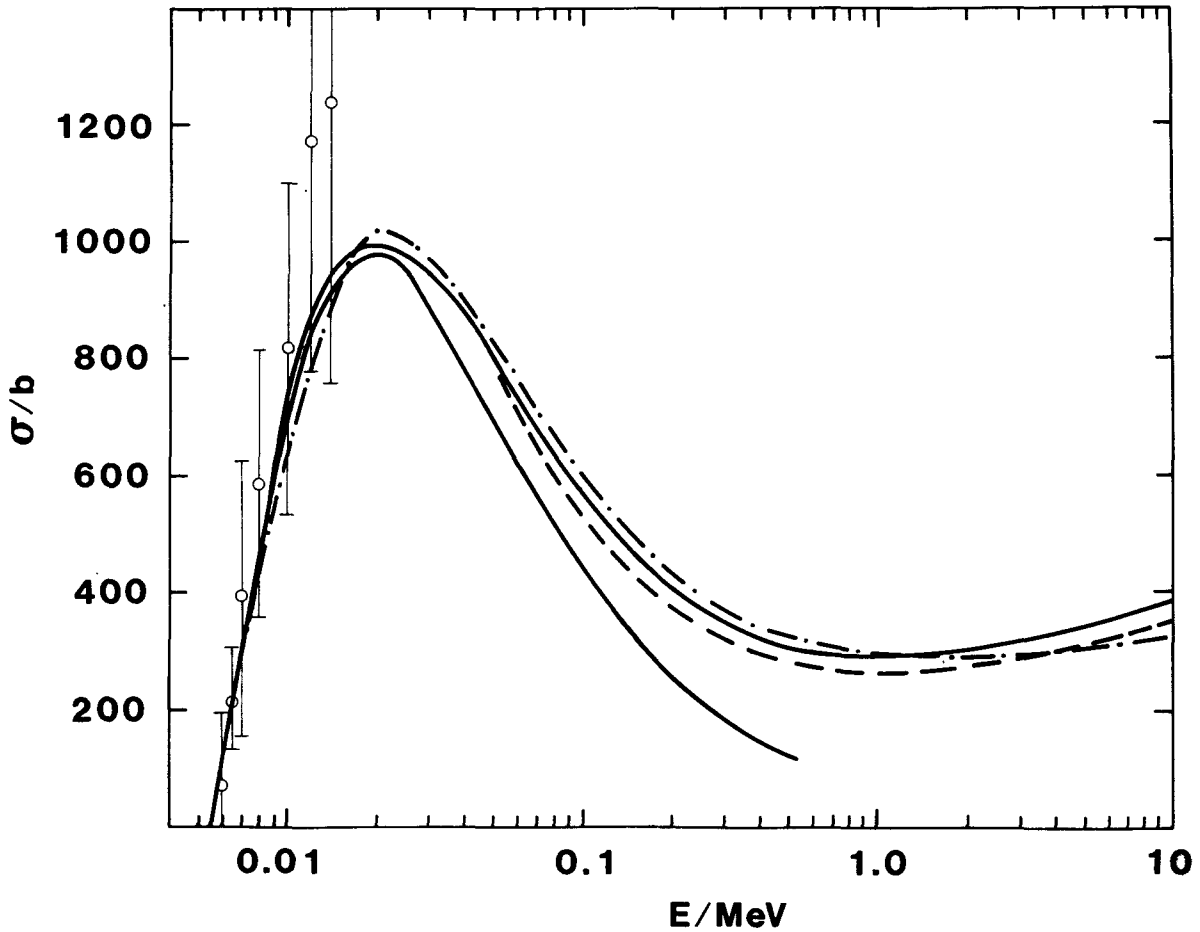

Fig. 6

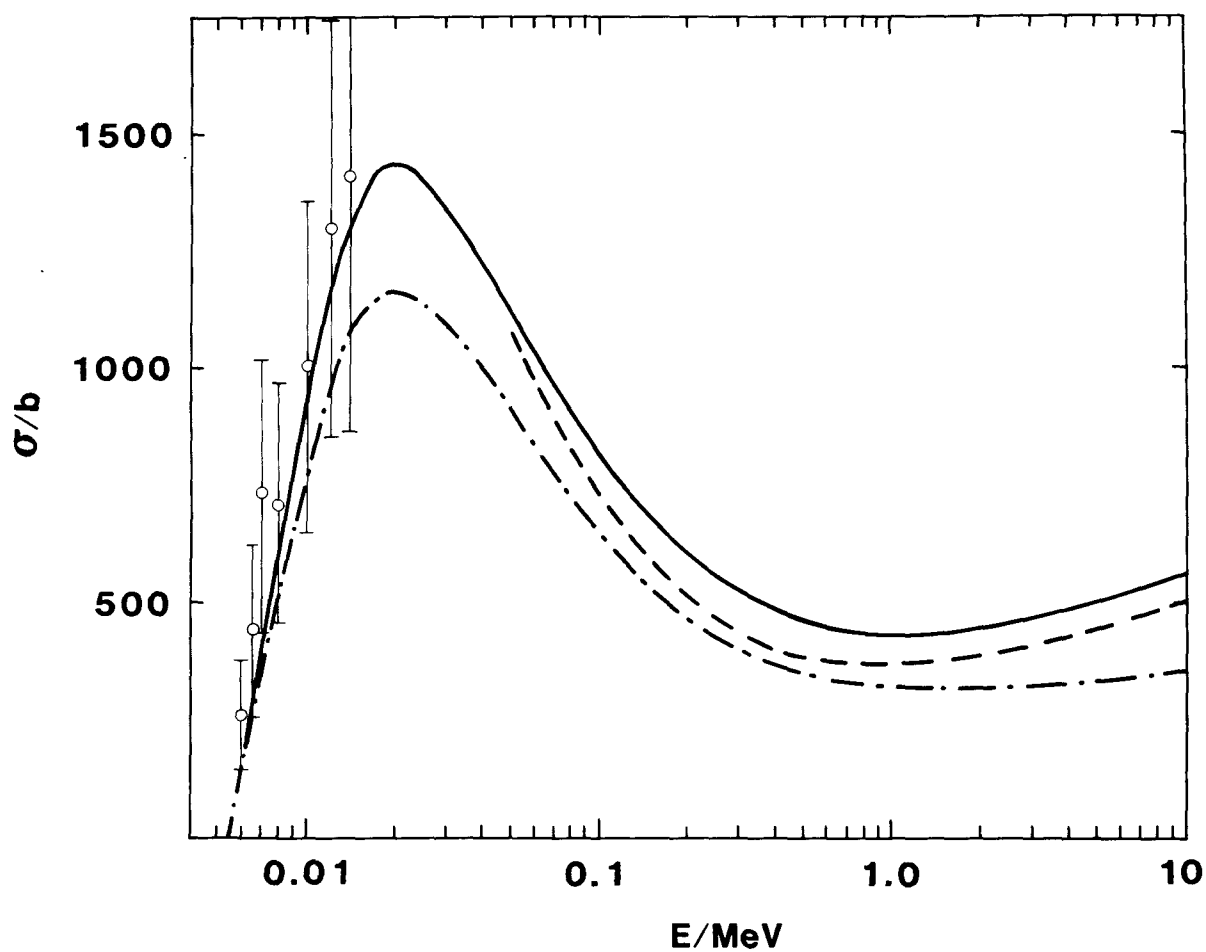

Fig. 7

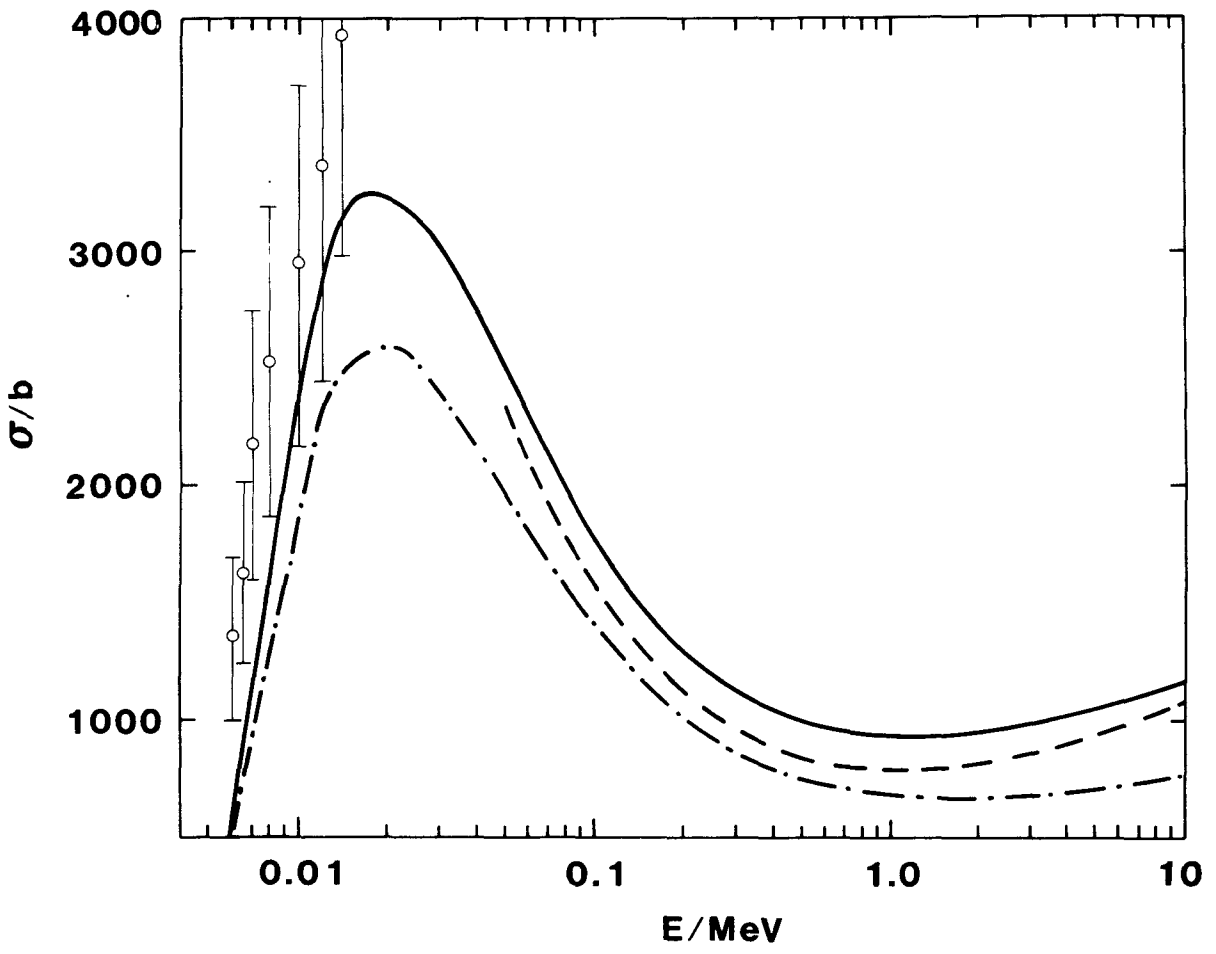

Fig. 8

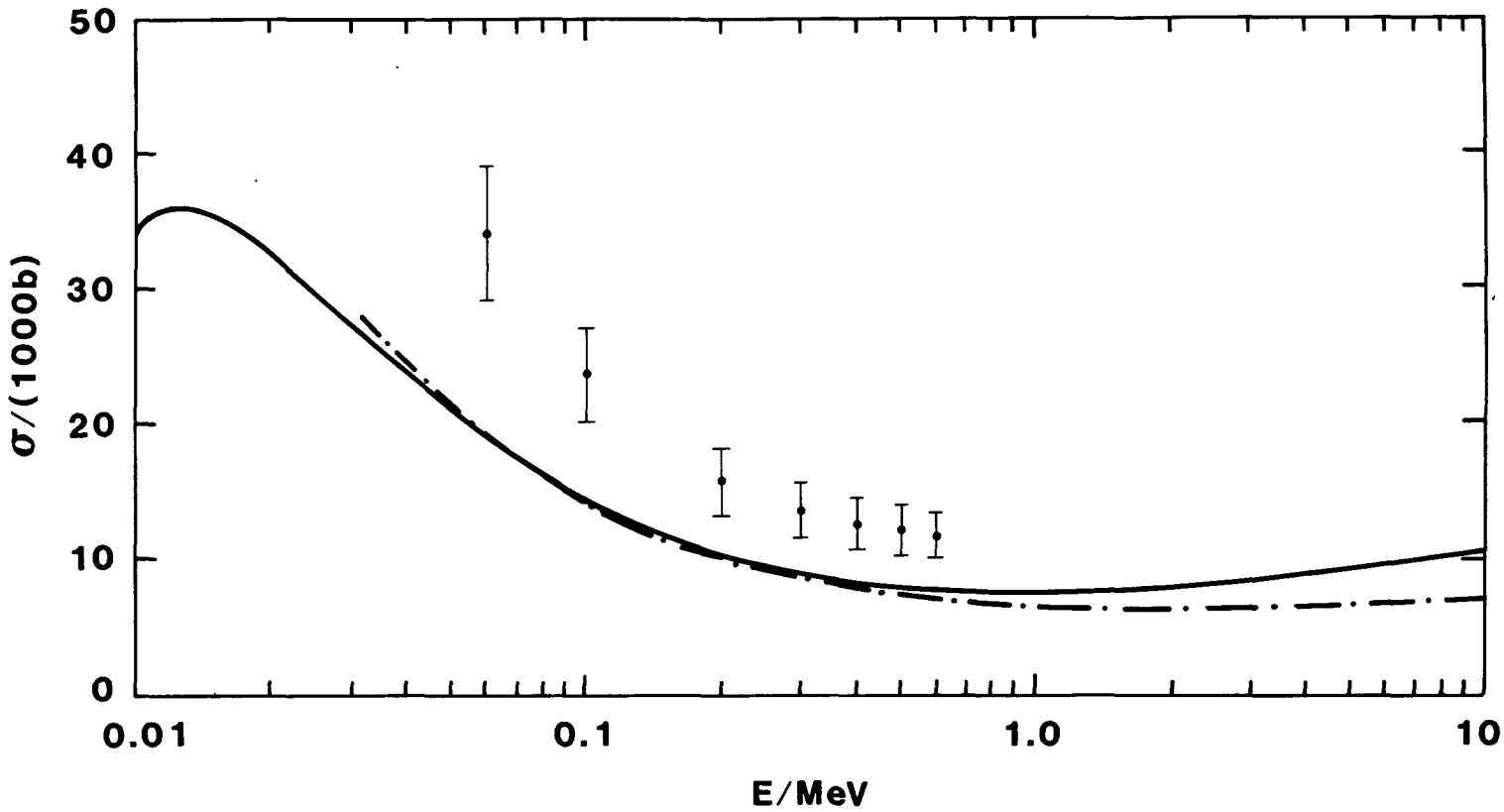

Fig. 9